Available online at www.sciencedirect.com
ScienceDirect
Acta Materialia 56 (2008) 3109–3119
Acta MATERIALIA
www.elsevier.com/locate/actamat

Atomistic simulations of the shear strength and sliding mechanisms of copper–niobium interfaces

J. Wang [a,*], R.G. Hoagland [a], J.P. Hirth [a], A. Misra [b]

[a] Materials Science and Technology Division, Materials Physics and Applications Division, Los Alamos National Laboratory, Los Alamos, NM 87545, USA
[b] Center for Integrated Nanotechnologies, Materials Physics and Applications Division, Los Alamos National Laboratory, Los Alamos, NM 87545, USA

Received 10 January 2008; received in revised form 29 February 2008; accepted 1 March 2008
Available online 11 April 2008

Abstract

Interfaces play a prominent role in the deformation behavior of high-strength Cu–Nb layered composites by acting as barriers to slip transmission due to core spreading of glide dislocations within interfaces. The dislocation core spreading along the interfaces implies these interfaces are weak in shear. In this investigation, we have used atomistic simulations to explore the shear resistance and sliding mechanism of interfaces of Cu–Nb layered composites, as a function of applied in-plane shear direction and different interface atomic structures. The simulation results indicate that the shear strengths of Cu–Nb interfaces are: (i) lower than the theoretical estimates of shear strengths for perfect crystals, (ii) strongly anisotropic, (iii) spatially non-uniform and (iv) strongly dependent on the atomic structures of interfaces. The mechanism of interface sliding involves glide of interfacial dislocation loops that nucleate in the weakest regions of interfaces.

Keywords: Molecular statics simulations; Slip; Dislocation; Interfaces; Multilayers

1. Introduction

Nanolayered metallic composites have been studied extensively due to the high hardness achieved in these material systems [1–3]. Recently, it has been shown that certain nanolayered composites, such as Cu–Nb, exhibit remarkable thermomechanical stability, in addition to ultra-high strengths and good ductility, at individual layer thicknesses of less than approximately 100 nm [4–7]. Experiments on sputter-deposited Cu–Nb multilayers have revealed that both the layered morphology and the interface crystallography are preserved after annealing in vacuum at temperatures of about $0.8T_m$ (T_m = melting point of Cu) [4], after severe plastic deformation via cold rolling [5,6] and after helium ion irradiation at ambient as well as at elevated temperatures [7].

At layer thicknesses below approximately 5 nm, the hardness of metallic multilayers reaches a maximum and, to a first order, is independent of the layer thickness [1,2]. Dislocation pile-up based mechanisms are not applicable at these length scales and the critical unit process in the deformation behavior is the transmission of single dislocations across interfaces. Atomistic modeling has been used by Hoagland et al. [8–10] to gain insight into slip transmission across bimetallic interfaces. For the case of Cu–Nb, this work [9,10] showed that the interfacial shear strength, in one direction, is relatively low. A consequence of this relatively low shear strength is that the stress field of a glide dislocation approaching the interface locally shears the interface, resulting in dislocation absorption and core spreading in the interface plane. It is extremely difficult for a lattice glide dislocation to compact its core in the

* Corresponding author. Tel.: +1 505 664 0696.
E-mail address: wangj6@lanl.gov (J. Wang).

1359-6454/$34.00 © 2008 Acta Materialia Inc. Published by Elsevier Ltd. All rights reserved.
doi:10.1016/j.actamat.2008.03.003

interface plane so that it can be emitted in the next layer [11]. This indicates that the interface barrier to slip transmission depends on the extent of core spreading in the interface plane, which, in turn, depends on the shear resistance of the interface. The dependence of the interface shear strength on the atomic structure of the interface was not investigated in the earlier work.

In this investigation, we have determined the variation in shear strength with respect to applied shear direction in the interface plane, for two different atomic structures [11] (described in the next section) that were observed for the same crystallographic orientation relationship between Cu and Nb. The shear strength of interfaces is defined as the critical shear stress at which irreversible sliding is induced along the interface. For the simplest case of a flat planar boundary with normal parallel to the y-axis, only two components of shear displacement need to be considered, along the x and z directions. The y-component of shear displacement is not treated as a variable since energies are minimized with respect to specific boundary volume, causing this component to be fixed. In addition, the shear–tension coupling effect is not considered, although the sliding strength of an interface depends on tension or compression normal to the boundary plane [12].

For the results shown in this paper, the atomic structures of the Cu–Nb interfaces are described in Section 2. The computational methodology to determine the shear resistance is described in Section 3. Shear strength and sliding mechanisms of interfaces are reported, respectively, in Sections 4 and 5. Finally, our conclusions are listed in Section 6.

2. Atomic structures of Cu–Nb interfaces

The atomic structure of a bimetallic interface may depend not only on thermodynamic variables but also on geometric factors [13]. A bilayer model of Cu and Nb is created and assembled from two unrelaxed semi-infinite perfect crystals with a Kurdjumov–Sachs (KS) epitaxial orientation relation so that $(1\,1\,1)_{Cu}\|(1\,1\,0)_{Nb}$ and $\langle 1\,\bar{1}\,0\rangle_{Cu}\|\langle\bar{1}\,1\,1\rangle_{Nb}$ [13]. Furthermore, it follows from the KS orientation relation that $[1\,1\,\bar{2}]_{Cu}$ is parallel to $[1\,\bar{1}\,2]_{Nb}$. For the same KS orientation relationship, our atomistic simulations have identified two possible atomic structures of Cu–Nb interfaces with approximately the same formation energy [15]. The first atomic structure, referred to as KS_1, is formed by directly combining two semi-infinite perfect crystals according to the KS orientation relationship [8]. The relaxed KS_1 configuration contains distinct patches where interface atoms of Cu and Nb have low coordination. The second atomic structure, referred to as KS_2, is formed by inserting a strained monolayer of Cu $\{1\,1\,1\}$ as an intermediate layer between the adjoining crystals in the KS_1 interface. This inserted monolayer, a perfect Cu $\{1\,1\,1\}$ plane, is strained in a way that removes patches of undercoordination present in a KS_1 interface [15], thereby stabilizing the interface configuration even though it contains a strained Cu monolayer.

Fig. 1 shows the bilayer model construction for the KS_1 interface, containing two parts: the moveable region 1 inside the simulation cell and the semi-rigid region 2 surrounding region 1. The heights of Cu and Nb crystals in the y-direction are chosen to be 6 nm each. The semi-rigid region acts as a fixed boundary during relaxation once the shear strain is applied. The thickness of semi-rigid region in the y-direction is 1 nm (twice the cut-off distance of the interatomic potential) for the two crystals. The periodic boundary conditions are applied in the x and z directions. The two dimensions in the x and z directions are not arbitrarily chosen because of the incommensurate nature of the Cu and Nb crystals, but determined such that the strains imposed on Cu and Nb semi-infinite perfect crystals are minimized and to ensure periodic boundary conditions and equilibrium of the bilayer composites. Cu crystal has 42 periodicity-lengths along $\frac{a_{Cu}}{2}[1\,1\,\bar{2}]_{Cu}$, 185.9530 Å, and 19 periodicity-lengths along $\frac{a_{Cu}}{2}[1\,\bar{1}\,0]_{Cu}$, 48.5677 Å; Nb crystal has 23 periodicity-lengths along $a_{Nb}[1\,\bar{1}\,2]_{Nb}$, 185.9614 Å, and 17 periodicity-lengths along $\frac{a_{Nb}}{2}[\bar{1}\,1\,1]_{Nb}$, 48.5958 Å. Equilibrium implies that normal stresses σ_{yy} in the two crystals are zero; the summation of stress σ_{zz} in the two crystals and the summation of stress σ_{xx} in the two crystals are zero. Periodicity requires equal dimensions in the x and z directions for the two crystals. The final dimension, solved from the six conditions, in the x direction is 185.956 Å, and in the z direction, 48.577 Å. The required strains are: $\varepsilon_{xx}^{Cu} = 0.3657e-4, \varepsilon_{yy}^{Cu} = -0.7963e-4$, $\varepsilon_{zz}^{Cu} = 0.1899e-3$, and $\varepsilon_{xx}^{Nb} = -0.8235e-5, \varepsilon_{yy}^{Nb} = 0.2762e-3$, $\varepsilon_{zz}^{Nb} = -0.3899e-3$; other strains not mentioned are zero.

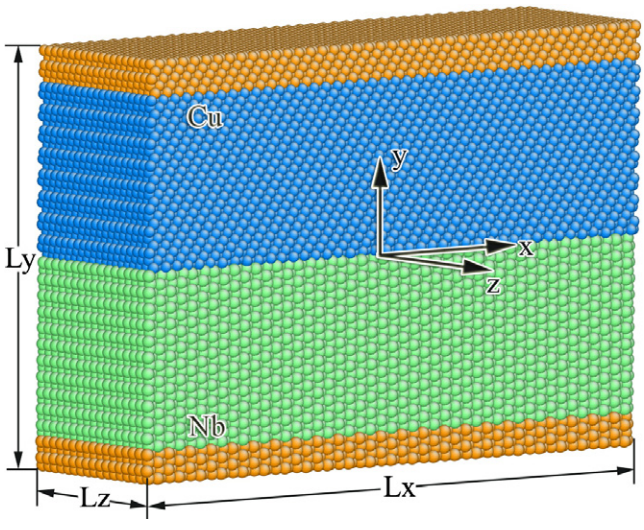

Fig. 1. Simulation cell, showing region 1 which is the movable part containing Cu atoms (blue) in the upper crystal and Nb atoms (green) in the lower crystal, and region 2 which is the semi-rigid part (yellow) surrounding region 1. Bilayer models have Kurdjumov–Sachs (KS) orientation relation: $(1\,1\,1)_{Cu}\|(1\,1\,0)_{Nb}\|$interface $-$ plane and $\langle 1\,\bar{1}\,0\rangle_{Cu}\|\langle\bar{1}\,1\,1\rangle_{Nb}$. Also, x $= [1\,1\,\bar{2}]_{Cu}$, y $= [1\,1\,1]_{Cu}$, and z $= [1\,\bar{1}\,0]_{Cu}$. (For interpretation of the references to color in this figure legend, the reader is referred to the web version of this article.)

Inserting a strained Cu monolayer in the KS_1 model described above creates the KS_2 interface structure. The strained Cu monolayer is constructed by applying displacement gradients $\partial u/\partial x = -0.04785$, $\partial u/\partial z = -0.09209$, $\partial w/\partial x = 0.02763$, $\partial w/\partial z = 0.05317$ to a perfect Cu {1 1 1}. In order to ensure periodicities in the x and z directions, this strained Cu monolayer is also subjected to additional displacement gradients, $\partial u/\partial x = -0.4144\text{e}{-4}$, $\partial u/\partial z = 0.4867\text{e}{-3}$, $\partial w/\partial x = -0.1441\text{e}{-4}$, $\partial w/\partial z = 0.8811\text{e}{-4}$. These additional displacement gradients are very small and comparable in magnitude to the strains originally imposed on the bulk Cu and Nb crystals to ensure periodicities in the x and z directions. The resulting interfacial monolayer has a lower atomic density: 0.995 less than the original perfect Cu {1 1 1}. It is worth emphasizing that the overall KS orientation relation is preserved between the adjoining Cu and Nb crystals, although the strained Cu monolayer does not form the KS orientation relation with Nb crystal.

Relaxation of the bilayer model is accomplished by the quenching molecular dynamics method. Embedded atom method (EAM) potentials are used for Cu [16] and Nb [17]. These potentials have produced good results for surface diffusion and defect formation energies [18–20]. The interaction potentials of Cu and Nb were constructed based on the lattice constant and bulk modulus of a hypothetical CuNb crystal in the CsCl structure [14]. This newly constructed potential has been used to study atomic structures of the Cu–Nb interface [10,11,15,21] and the growth mechanism of Cu–Nb layered composites during physical vapor deposition [22]. During the relaxation, the two crystals are able to translate in three directions, but rotation is not allowed. In case the relaxation is trapped at a local minimum energy, two steps are undertaken. First, the two crystals are allowed to translate in three directions with respect to each other as rigid bodies, searching for the most favorable relative positions and interface spacing. In the case of the KS_2 interface, the strained Cu monolayer was also allowed to undergo independent rigid body translation. In the second relaxation step, the two crystals can translate in three directions and all atom positions are allowed to relax fully and independently until the maximum force acting on any atom does not exceed 5 pN. The net forces, acting parallel and perpendicular to the interface, drive the translations.

The atomic structures of the KS_1 and KS_2 interfaces after relaxation are shown in Figs. 2 and 3, respectively. In this paper, the boundary between the Cu and Nb crystals in KS_1 is referred to as the Cu–Nb interface, the boundary between the Cu crystal and the strained Cu monolayer is referred to as the Cu–Cu^{α} interface, and the boundary between the strained Cu monolayer and the Nb crystal is referred to as the Cu^{α}–Nb interface. There are two distinctive features of KS_1 as compared to KS_2: (i) a quasi-repeating pattern corresponding to a two-dimensional boundary unit cell (shown by the parallelogram in Fig. 2a); and (ii) groups of atoms, contained within a circular region of about 15 Å in diameter, which

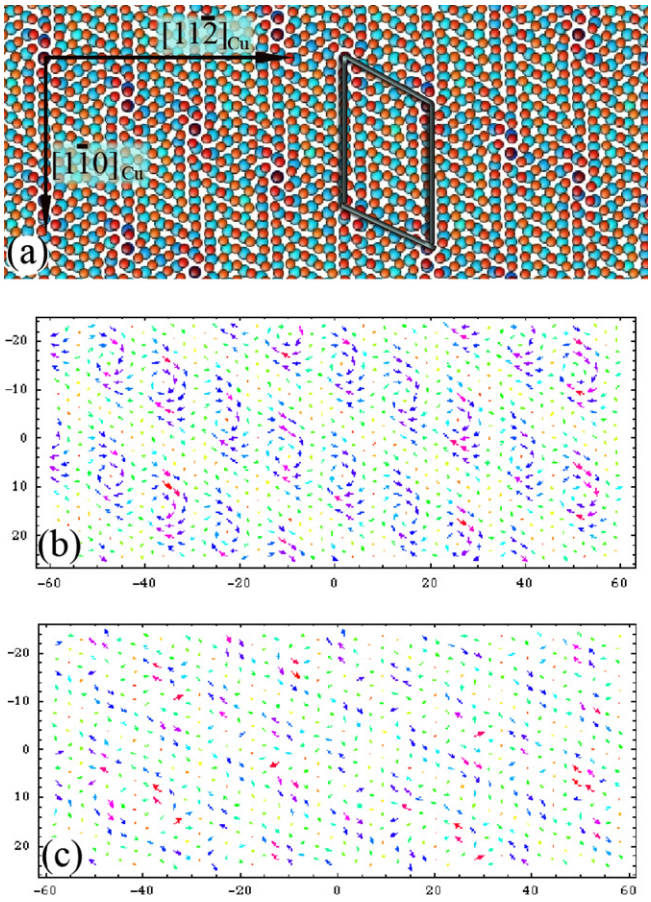

Fig. 2. Atomic structure of the KS_1 interface, showing (a) atoms in Cu and Nb crystals adjacent to a flat interface. Atoms are colored by their excess potential energy relative to their respective cohesive energies. Cu atom has positive excess energy (shown as red color), and Nb atom has negative excess energy (shown as green color). The in-plane displacements of (b) Cu atoms and (c) Nb atoms are relative to their initial positions in the perfect Cu and Nb crystals. (For interpretation of the references to color in this figure legend, the reader is referred to the web version of this article.)

undergo displacements tangential to the circle (Fig. 2b). The magnitudes of the displacements are zero at/near circle center and increase with increasing distance from the center, analogous to a vortex. As can be seen from Fig. 3b and c, both features do not appear in the KS_2 interfaces, but Cu atoms in some regions undergo large relative displacements.

3. Computational methodology for interfacial shear strength

The shear resistance of the interface is investigated with respect to different shear directions that are chosen based on the gamma surface [23]. The interface energy surfaces, i.e., gamma surfaces, are shown in Fig. 4a for KS_1, and in Fig. 4b–d for KS_2. These energy surfaces imply three preferred shear directions for KS_1, along $\langle 1\bar{1}0\rangle_{Cu}$, $\langle 1\bar{1}1\rangle_{Nb}$ and $\langle 100\rangle_{Nb}$, and two preferred shear directions for KS_2, along $\langle 10\bar{1}\rangle_{Cu}$ with respect to the translation of Cu crystal over the strained Cu monolayer, and $\langle 01\bar{1}\rangle_{Cu}$ with respect to the translation of the strained Cu monolayer over Nb

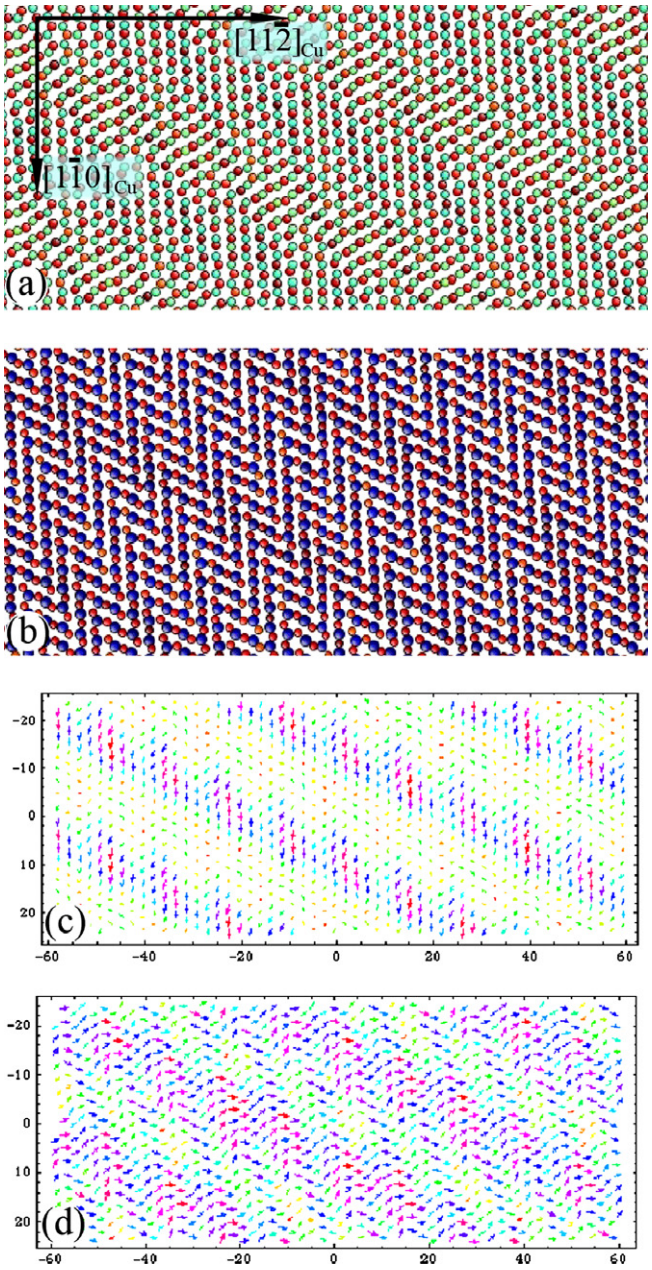

Fig. 3. Atomic structure of the KS_2 interface, showing (a) atoms in the strained Cu monolayer and the second Cu layer, and (b) atoms in the strained Cu monolayer and the first Nb layer. Atoms are colored by their excess potential energy relative to their respective cohesive energies. Cu atoms in the strained monolayer have positive excess energy (about 0.40 eV) (shown as red color), Cu atoms in the second Cu layer have positive excess energy (about 0.03 eV) (shown as green color), and Nb atoms in the first Nb layer have negative excess energy (shown as blue color). The in-plane displacements of Cu atoms, (c) in the second layer and (d) in the strained monolayer, are relative to their initial positions in perfect Cu crystal. (For interpretation of the references to color in this figure legend, the reader is referred to the web version of this article.)

crystal. In what follows we have applied homogeneous shears in six directions, three along $\langle 1\,1\,0\rangle_{Cu}$ and three along $\langle 1\,1\,2\rangle_{Cu}$. Although the two directions, $\langle 10\bar{1}\rangle_{Cu}$ and $\langle 0\,1\,\bar{1}\rangle_{Cu}$ are not exactly parallel to two directions of the preferred shear directions in KS_1, the offset is small: $\langle 1\,0\,\bar{1}\rangle_{Cu}$ is 5.5° from $\langle 1\,0\,0\rangle_{Nb}$.

A gradually increasing shear strain is applied homogeneously to bilayer models of Cu–Nb with the KS_1 and KS_2 interfaces along the six chosen shear directions while maintaining equilibrium, i.e., $\sigma_{yx}^{Cu} = \sigma_{yx}^{Nb}$ and $\sigma_{yz}^{Cu} = \sigma_{yz}^{Nb}$. The shear stresses σ_{yx} and σ_{yz} parallel to the interface are generated by applying the displacement gradients, $\partial u/\partial y$ and $\partial w/\partial y$, to the two crystals. u and w are the displacements along the x and z directions. Shearing of the two crystals is achieved by maintaining their ratio constant at every loading step. Because of the difference in shear moduli, the ratio of displacement gradients $\partial u/\partial y$ and $\partial w/\partial y$ to maintain equilibrium in the Nb crystal differs from that in Cu, and the increments of the displacement gradients also differ. The boundary conditions in the models were satisfied while departures from equilibrium were minimized by incrementing the displacement gradients such that the shear stress increments were less than 30 MPa at each loading step. The tolerance of 30 MPa is chosen to prevent overshooting the shear strength of interface when applying shear strain increments. After applying the displacement gradient increments to the two crystals, all atomic positions are then allowed to relax fully and independently. Taking the shear along the direction $\langle 1\,0\,\bar{1}\rangle_{Cu}$ as an example, shear stresses σ_{yx} and σ_{yz} are shown in Fig. 5a as a function of the loading steps. Under equilibrium, the shear stresses are equal in the two crystals during elastic shearing. However, at some loading steps, the shear stresses deviate from equilibrium. For example, once the interface shears locally, the shear stresses after the nth loading step are $\sigma_{yx}^{Nb} \neq \sigma_{yx}^{Cu}$ and $\sigma_{yz}^{Nb} \neq \sigma_{yz}^{Cu}$. The stress increments $\delta\sigma$ for the $(n+1)$th loading step are determined so that the bilayer composite is in equilibrium again, i.e. $\sigma_{yx}^{Nb} + \delta\sigma_{yx}^{Nb} = \sigma_{yx}^{Cu} + \delta\sigma_{yx}^{Cu}$ and $\sigma_{yz}^{Nb} + \delta\sigma_{yz}^{Nb} = \sigma_{yz}^{Cu} + \delta\sigma_{yz}^{Cu}$. The displacement gradient increments for the $(n+1)$th loading step are solved according to Hooke's law.

Fig. 5b shows an example of the effective shear stress as a function of the effective shear strain with respect to the shear along $\langle 1\,0\,\bar{1}\rangle_{Cu}$ for KS_1. Initially, the effective shear stress increases linearly up to an effective shear strain of 2.3%. Continued shear causes irreversible sliding along the interface and the effective shear stress fluctuates within a range. The average between the maximum and minimum stresses is adopted as the shear resistance, which in this case is 1.04 GPa.

During shearing of the two crystals, disregistry analysis was used to determine slip in interface. In this analysis, pairs of atoms across the desired shear plane are first identified in a reference, relaxed system. The displacements of these atoms in the sheared system are determined with respect to the reference system. Disregistry is the difference of the displacements of atoms in each pair identified in the reference, relaxed system.

4. Shear response of interfaces

Shear resistance and shear response of both the KS_1 and KS_2 interfaces were investigated by applying a gradually increasing homogeneous shear strain to bilayer models of

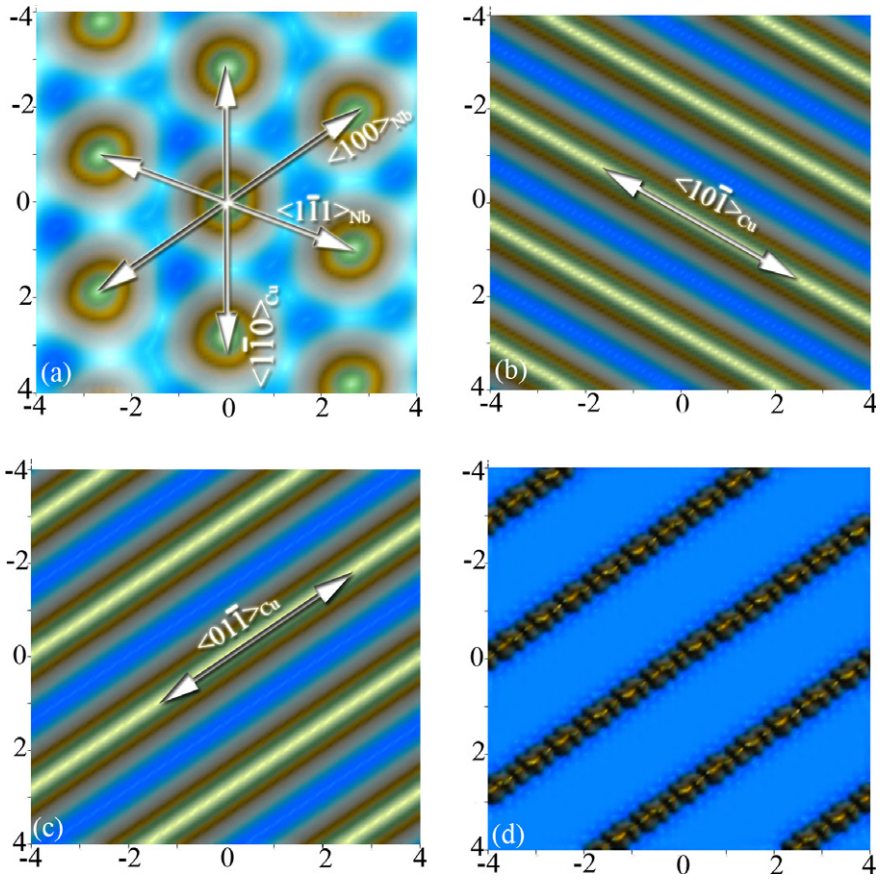

Fig. 4. Gamma surfaces corresponding to two-dimensional translation along interface of one crystal over the other: (a) Cu–Nb interface in KS_1, (b) Cu–Cu^{α} interface in KS_2 and (c) Cu^{α}–Nb interface in KS_2, and (d) the details of the interface in (c) as the high-energy region is removed. Arrowed lines indicate the preferred shear directions. High-energy regions are shown in blue and low-energy regions in green. The horizontal axis is along $[1\,1\,\bar{2}]_{Cu}$, the vertical axis is along $[1\,\bar{1}\,0]_{Cu}$, and both have units of angstroms. (For interpretation of the references to color in this figure legend, the reader is referred to the web version of this article.)

Cu–Nb with respect to the six chosen shear directions. The results are summarized below.

4.1. KS_1 interface

With respect to the six shear directions, shear resistances are summarized in Table 1. The KS_1 interface has the strongest shear resistance, 1.1 GPa, for shear along $[1\,1\,\bar{2}]_{Cu}$, as shown in Fig. 6a. Fig. 6b shows the result of disregistry analysis at an effective shear strain of 4.0%. Two features are worth noting. First, slip in the non-vortex region is not along the applied shear direction, but along $[0\,1\,\bar{1}]_{Cu}$, implying that the non-vortex region has a relative easy shear direction along $[0\,1\,\bar{1}]_{Cu}$. As a result, the shear stress σ_{yz} is not zero (Fig. 6c) as shear stress σ_{yx} exceeds 0.20 GPa, although only one non-zero displacement gradient, $\partial u/\partial y$, is applied. Second, the sliding distance in the vortex regions is longer than that in the non-vortex regions, implying that the shear resistance is spatially non-uniform. The vortex region has lower shear resistance than the non-vortex region.

With respect to applied strain along $[\bar{1}\,2\,\bar{1}]_{Cu}$, the KS_1 interface has the weakest shear resistance, 0.40 GPa (Fig. 7a). The slip directions in both the vortex and the non-vortex regions deviate slightly from the applied shear direction, and again, slip in the non-vortex region is along the preferred shear direction $[0\,1\,\bar{1}]_{Cu}$, as shown in Fig. 7b. The preferred shear direction $[0\,1\,\bar{1}]_{Cu}$ in the non-vortex region is also revealed in shear studies of the interface along different applied shear directions, such as shearing the two crystals along $[1\,\bar{1}\,0]_{Cu}$ as shown in Fig. 8a. However, the shear resistance is not the lowest (0.49 GPa) with respect to the shear along $[0\,1\,\bar{1}]_{Cu}$, since slip in the vortex region is not along this direction but along $[\bar{1}\,2\,\bar{1}]_{Cu}$ (Fig. 8b).

Slip always seems to initiate in the vortex region and the sliding direction in the vortex region is along the applied shear direction. This implies that the vortex region has lower shear resistance than the non-vortex region. The detailed mechanisms of atomic-scale sliding in interfaces will be discussed in the next section.

4.2. KS_2 interfaces

Shear strengths for applied strain along six different directions are summarized in Table 1. The strongest shear resistance is 0.18 GPa for applied strain along the preferred shear direction $[0\,1\,\bar{1}]_{Cu}$ in the Cu^{α}–Nb interface, and the

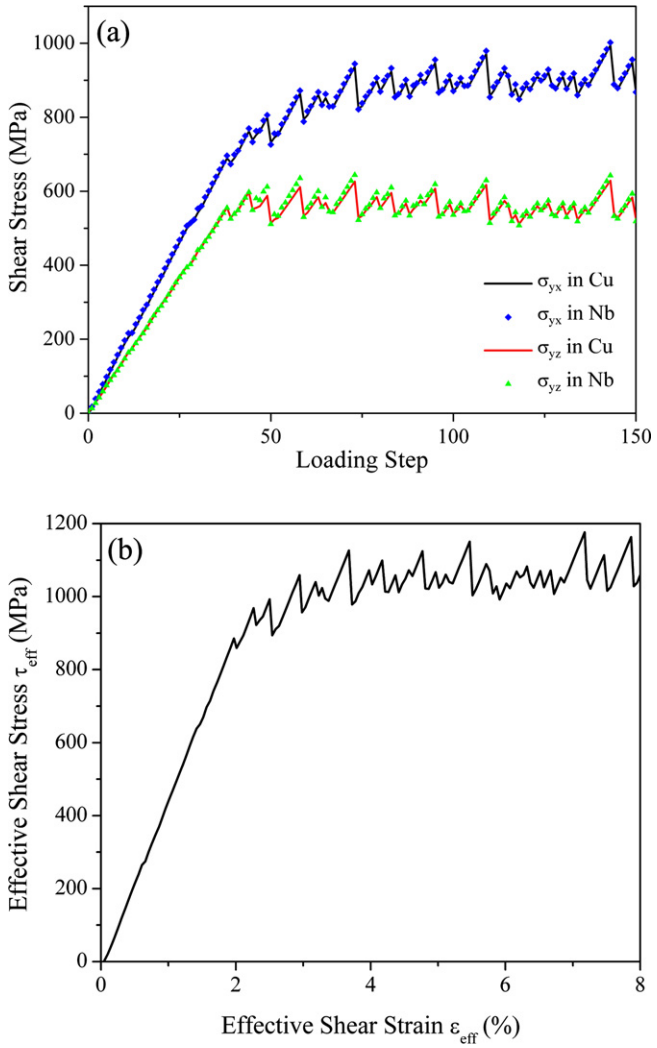

Fig. 5. Shear stress with respect to strain for the shearing direction of $[1\,0\,\bar{1}]_{Cu}$ for KS_1, showing (a) shear stresses σ_{yx} and σ_{yz} in the two crystals Cu and Nb as a function of loading steps, and (b) the effective shear stress–strain curve.

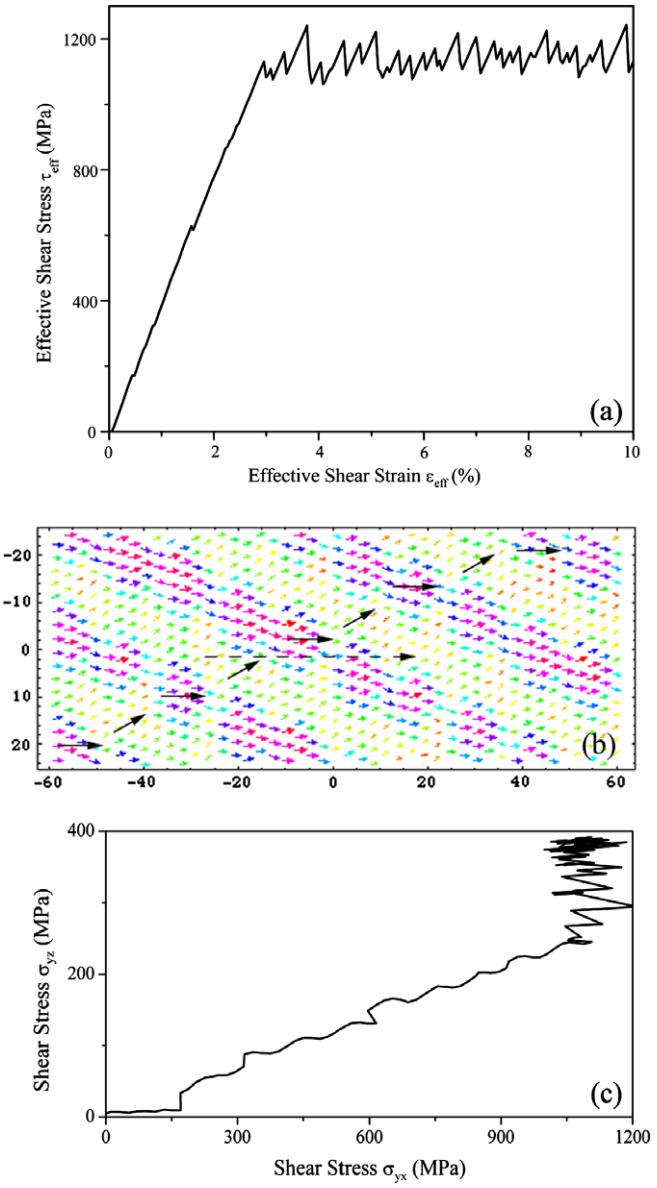

Fig. 6. Shear response of the KS_1 interface with respect to applied strain along $[1\,1\,\bar{2}]_{Cu}$, showing (a) the effective shear stress–strain curve, (b) the vector plot of disregistry at the effective shear strain of 4.5%, and (c) shear stresses σ_{yx} and σ_{yz} associated with continued shear of the two crystals. The dashed arrowed line indicates the applied shear direction, and black arrows show the local sliding directions.

weakest shear resistance is 0.06 GPa along the preferred shear direction $[1\,0\,\bar{1}]_{Cu}$ in the Cu–Cu^{α} interface. It is worth mentioning that slip only occurs in the Cu–Cu^{α} interface (Fig. 9a) for applied strain along $[1\,0\,\bar{1}]_{Cu}$, but for other directions, slip is observed at both the Cu–Cu^{α} and Cu^{α}–Nb interfaces. This indicates that the shear resistance of the Cu–Cu^{α} interface is lower than that of the Cu^{α}–Nb interface. For example, Fig. 9b shows that slip occurs at both interfaces, i.e. Cu^{α}–Nb along the preferred shear direction $\langle 0\,1\,\bar{1}\rangle_{Cu}$, and Cu–$Cu^{\alpha}$ along the preferred shear direction $\langle 1\,0\,\bar{1}\rangle_{Cu}$, for applied strain along $[1\,\bar{1}\,0]_{Cu}$. Both sliding directions are not parallel to the applied shear direction. As a result, the shear stress σ_{yx} is not zero (Fig. 9c) after the shear stress σ_{yz} exceeds 0.14 GPa, although the two crystals are only subjected to one non-zero displacement gradient $\partial w/\partial y$. Again, the lower shear resistance in

Table 1
Shear strengths (GPa) of Kurdjumov–Sachs oriented Cu–Nb interfaces for different applied in-plane shear directions for two different atomic structures, KS_1 and KS_2

Shear direction	$[1\,\bar{1}\,0]_{Cu}$	$[2\,\bar{1}\,\bar{1}]_{Cu}$	$[1\,0\,\bar{1}]_{Cu}$	$[1\,1\,\bar{2}]_{Cu}$	$[0\,1\,\bar{1}]_{Cu}$	$[\bar{1}\,2\,\bar{1}]_{Cu}$
KS_1	0.63	0.81	1.04	1.10	0.49	0.40
KS_2	0.15	0.11	0.06	0.11	0.18	0.16

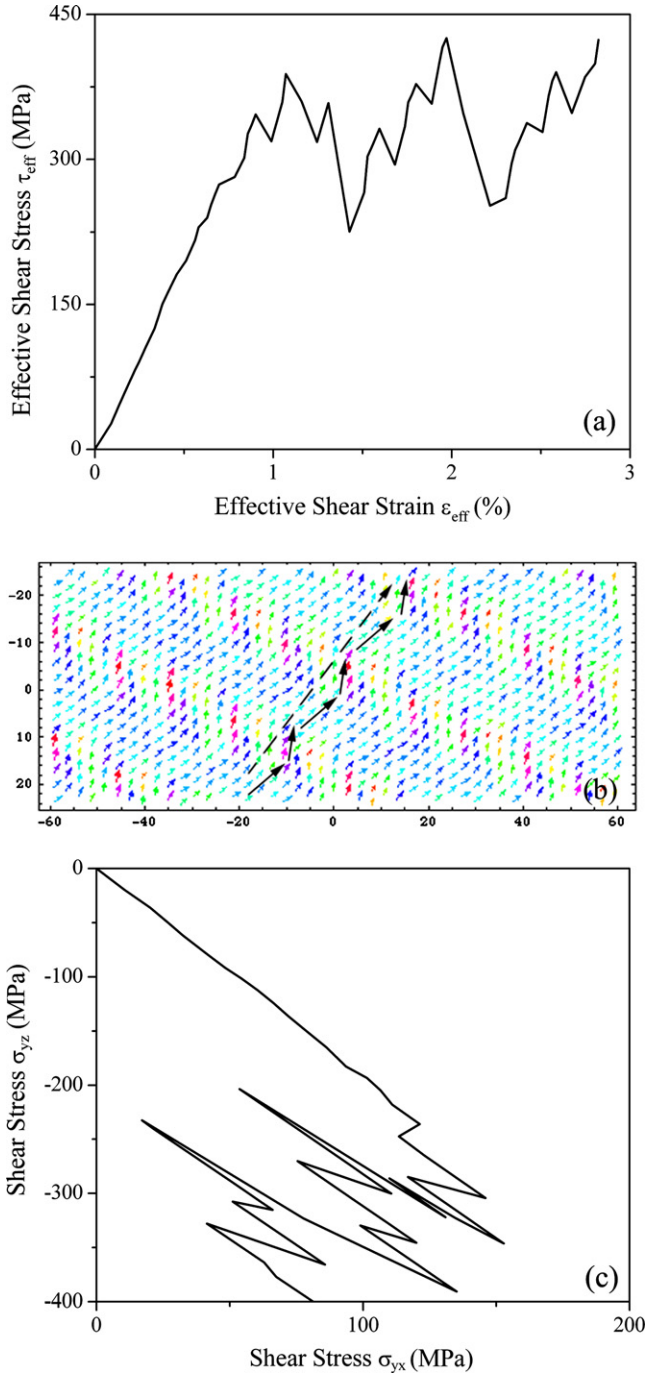

Fig. 7. Shear response of the KS_1 interface with respect to shear along $[\bar{1}2\bar{1}]_{Cu}$, showing (a) the effective shear stress–strain curve, (b) the vector plot of disregistry at the effective shear strain of 2.5%, and (c) shear stresses σ_{yx} and σ_{yz} associated with continued shear the two crystals. In (b), the dashed arrowed line indicates the applied shear direction, and black arrows show the local sliding directions.

the Cu–Cu$^{\alpha}$ interface is revealed with respect to shear along $[2\bar{1}\bar{1}]_{Cu}$. Fig. 10a shows that shear stresses initially increase, corresponding to the applied shear direction. When slip occurs, the shear stress σ_{yx} changes its sign to be negative, implying that the shear strain ε_{yx} induced due to slip is larger than the applied shear strain increment. The induced shear strain ε_{yx} is attributed to slip in the Cu–Cu$^{\alpha}$ interface

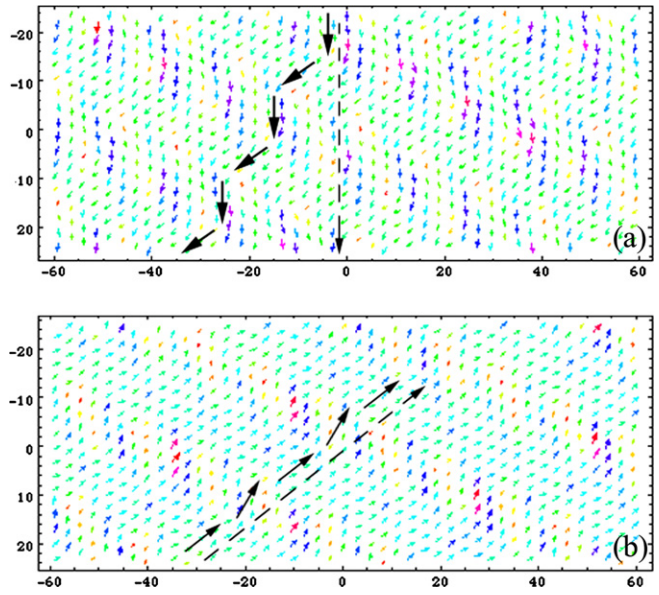

Fig. 8. The vector plot of disregistry at the effective shear strain of 2.5% for the KS_1 interface with respect to shear along (a) $[1\bar{1}0]_{Cu}$ and (b) $[01\bar{1}]$. The dashed arrowed line indicates the applied shear direction, and black arrowed lines show the local sliding directions in the vortex region and the non-vortex region.

parallel to $\langle 10\bar{1}\rangle_{Cu}$, as shown in Fig. 10b. Slip occurs in the Cu$^{\alpha}$–Nb interface along the direction diverging from $\langle 01\bar{1}\rangle_{Cu}$ by about 10°.

It is also noticed that shear resistance at both the Cu–Cu$^{\alpha}$ and Cu$^{\alpha}$–Nb interfaces is spatially non-uniform. As shown in Figs. 9a, b and 10b, the sliding distance in the large displacement region is longer than that in other regions. Slip always initiated in the large displacement region regardless of the applied strain direction, implying lower shear resistance in this region.

4.3. Comparison of shear responses of KS_1 and KS_2

The shear resistances of the KS_1 and KS_2 interfaces for different in-plane straining directions are plotted in Fig. 11. Two important features should be noted: (i) both the KS_1 and KS_2 interfaces have significantly lower shear resistance than the theoretical shear strengths estimated for the glide planes of either Cu or Nb defect-free single crystals; and (ii) Shear resistance is strongly anisotropic. For KS_1, the strongest shear resistance of 1.1 GPa corresponds to the shear along $\langle 11\bar{2}\rangle_{Cu}$, and the weakest shear resistance of 0.4 GPa is along $\langle 2\bar{1}\bar{1}\rangle_{Cu}$. For KS_2, the strongest shear resistance, 0.18 GPa, corresponds to shear along $\langle 01\bar{1}\rangle_{Cu}$, and the weakest shear resistance, 0.06 GPa, is for applied strain along $\langle 10\bar{1}\rangle_{Cu}$.Details of the atomic-scale sliding at interfaces are revealed by disregistry analysis. When the applied shear stress reaches the critical stress level needed to induce irreversible sliding along interfaces, sliding occurs only at the Cu–Nb interface for KS_1, but on the two interfaces for KS_2, Cu–Cu$^{\alpha}$ and Cu$^{\alpha}$–Nb interfaces. Furthermore, the shear resistance is spatially non-uniform in

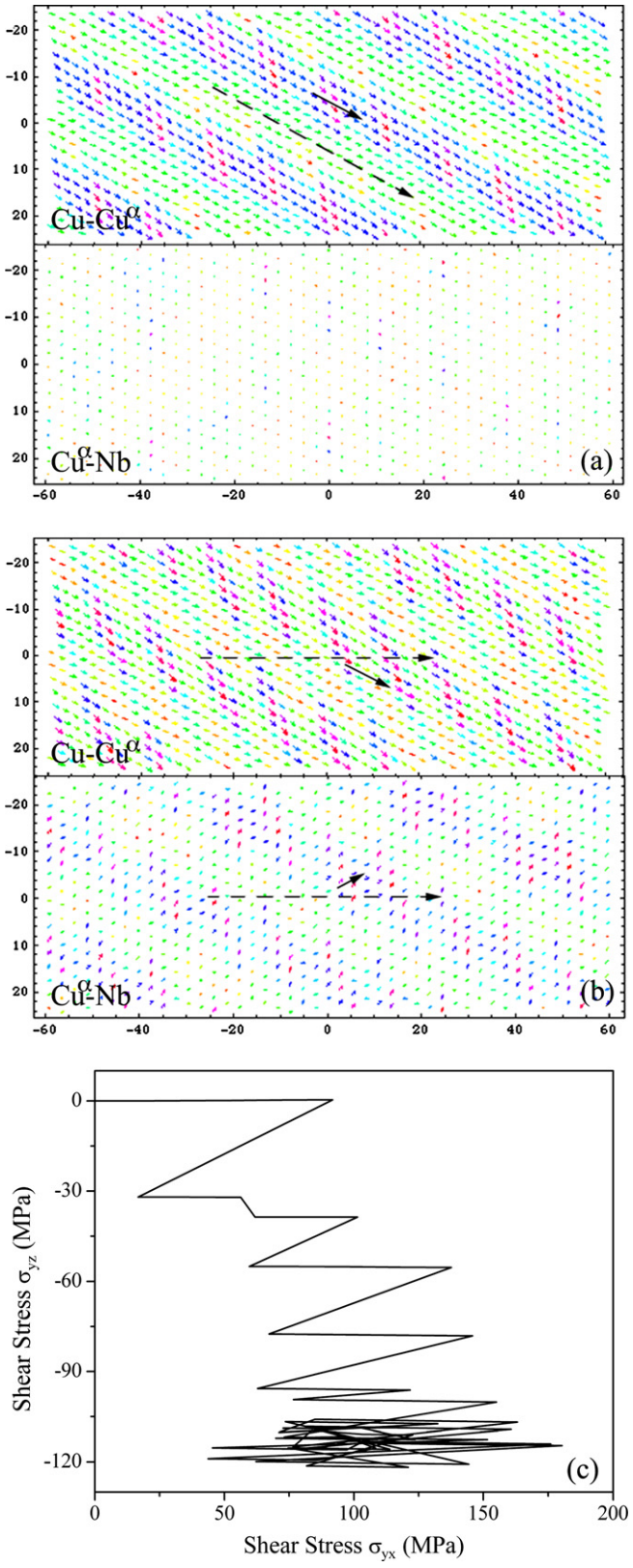

Fig. 9. Shear response of the KS_2 interface, showing the vector plot of disregistry at the effective shear strain of 2% for applied strain along (a) $[10\bar{1}]_{Cu}$ and (b) $[11\bar{2}]_{Cu}$. The dashed arrowed line indicates the applied shear direction, and black arrowed lines show the local sliding directions. (c) Evolution of shear stresses σ_{yx} and σ_{yz} associated with the continued shearing of the two crystals along $[1\,1\,\bar{2}]_{Cu}$.

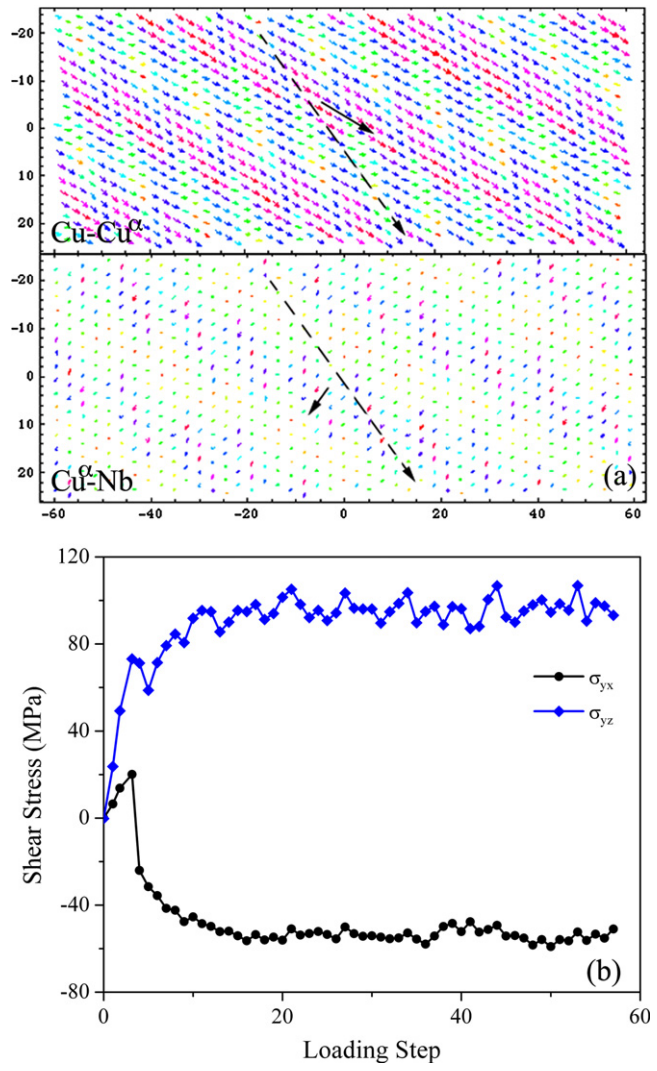

Fig. 10. Shear response of the KS_2 interface, showing (a) the vector plot of disregistry at the effective shear strain of 2% for applied strain along $[2\,\bar{1}\,\bar{1}]_{Cu}$, and (b) evolution of shear stresses σ_{yx} and σ_{yz} associated with the continued shearing of the two crystals. The dashed arrowed line indicates the applied shear direction, and black arrowed lines show the local sliding directions.

both interfaces. Irreversible sliding occurs non-uniformly, beginning within the vortex regions in the KS_1 interface and the large displacement regions in the KS_2 interface. As sliding commences, dislocations are formed, separating the slipped and non-slipped regions. These two important features are described in more detail in the following section.

5. Interface sliding mechanism

The spatially non-uniform sliding in the interface suggests an interface sliding mechanism in which dislocation loops nucleate in interfaces and subsequently expand by gliding in the interface plane. For KS_1, dislocation loops nucleate initially in the weakest regions of the Cu–Nb interface. For example, Fig. 12a–d show the disregistry evolu-

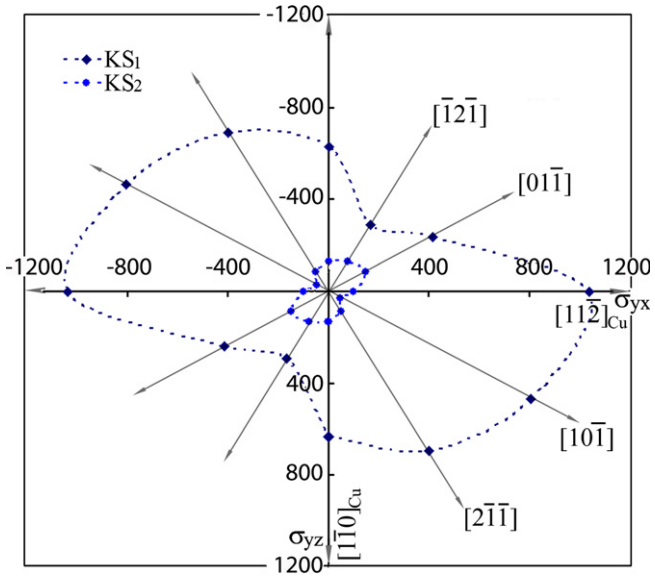

Fig. 11. Two-dimensional flow stress diagram for both KS_1 and KS_2. The horizontal axis is the shear stress σ_{yx} (MPa), and the vertical axis is the shear stress σ_{yz} (MPa).

tion corresponding to the effective shear strains of 3.0, 3.5, 4.0 and 4.5%, respectively, when the applied shear direction is along $\langle 1\,0\,\bar{1}\rangle_{Cu}$. For convenience in describing the interface sliding, the dashed circles in Fig. 12a represent dislocation loops generated at the onset of sliding in the weak shear regions, and the dashed lines approximate the locations of interfacial dislocations, separating the slipped and non-slipped regions in the interface. As shear continues, the dislocation loops expand, coalesce and glide in the interface (Fig. 12b–d). Fig. 12c shows that the sliding direction is parallel to the dislocation lines, indicating that the interfacial dislocation is screw.

Similar behavior is observed for KS_2. Fig. 13a shows the effective shear stress–strain curve with respect to the shear along $\langle 1\,1\,\bar{2}\rangle_{Cu}$. Sliding occurs at two interfaces: the Cu–Cu^{α} interface and the Cu^{α}–Nb interface. For effective shear strains of 1.0% and 1.5%, Fig. 13b and c, respectively, show the vector plots of disregistry of the Cu–Cu^{α} interface and the Cu^{α}–Nb interface.

The sliding mechanism, involving dislocation loop nucleation, observed in the atomistic simulations of Cu–Nb interfaces is applicable for all in-plane shear directions in both KS_1 and KS_2 atomic structures. For KS_1, the sliding mechanism only operates in the Cu–Nb interface, but for KS_2, sliding is observed in the two parallel atomic planes: Cu–Cu^{α} and Cu^{α}–Nb. The interfacial sliding behavior is different from the homogeneous shear of perfect crystals in which dislocations cannot nucleate due to the uniform shear resistance in the applied shear plane.

6. Discussions and conclusions

Atomistic simulations were performed to elucidate the shear strengths and sliding mechanism of face-centered cubic (fcc)/body-centered cubic (bcc) interfaces. For the

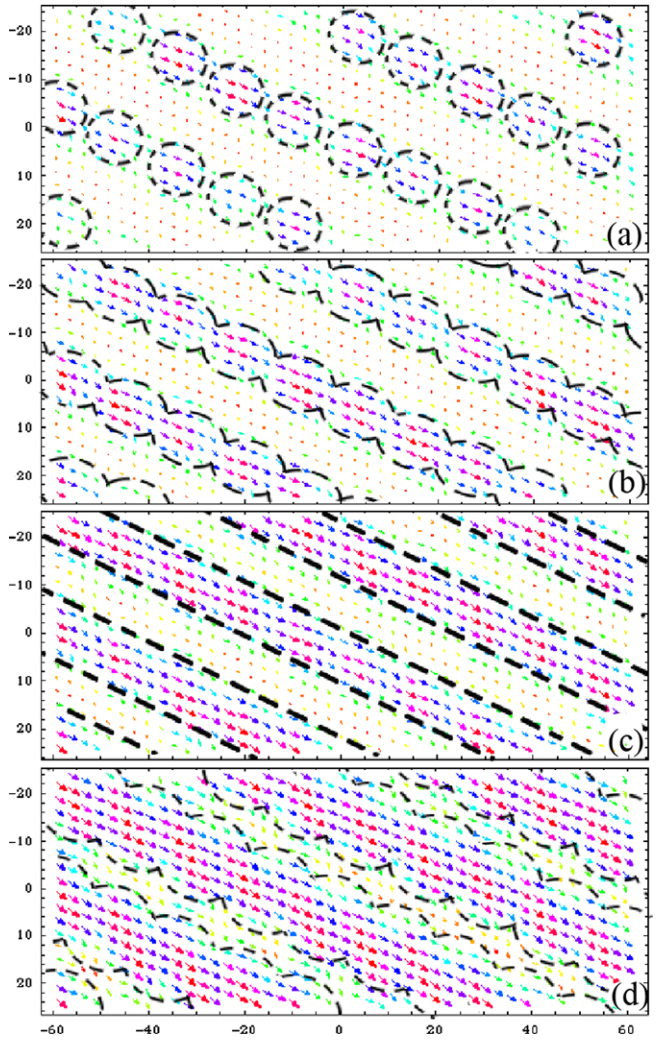

Fig. 12. Patterns in the vector plots of disregistry, showing the extent of interface sliding for KS_1 with respect to the applied shear direction $[1\,0\,\bar{1}]_{Cu}$, corresponding to different effective shear strains at (a) 3.0%, (b) 3.5%, (c) 4.0% and (d) 4.5%. Arrows show disregistry and dashed lines represent dislocations.

KS orientation relation, two different atomic arrangements (referred to as KS_1 and KS_2) are observed for Cu–Nb layered composites. The results revealed several important features.

First, interfaces of Cu–Nb layered composites have low shear strength. The stress field of a lattice glide dislocation approaching the interface is able to shear the interface, resulting in dislocation core spreading in the interfaces. The difference in shear resistance between KS_1 and KS_2 implies that core spreading will be wider in the KS_2 than in the KS_1 interface.

Second, irreversible sliding occurs only in the Cu–Nb interface for KS_1, but in two interfaces, Cu–Cu^{α} and Cu^{α}–Nb, for KS_2. This difference implies that the dislocation core will spread in two atomic layers for KS_2, making it more difficult for dislocations to cross the KS_2 interface than the KS_1 interface.

Third, shear resistance is spatially non-uniform in interfaces. This spatial non-uniformity plays a prominent role on

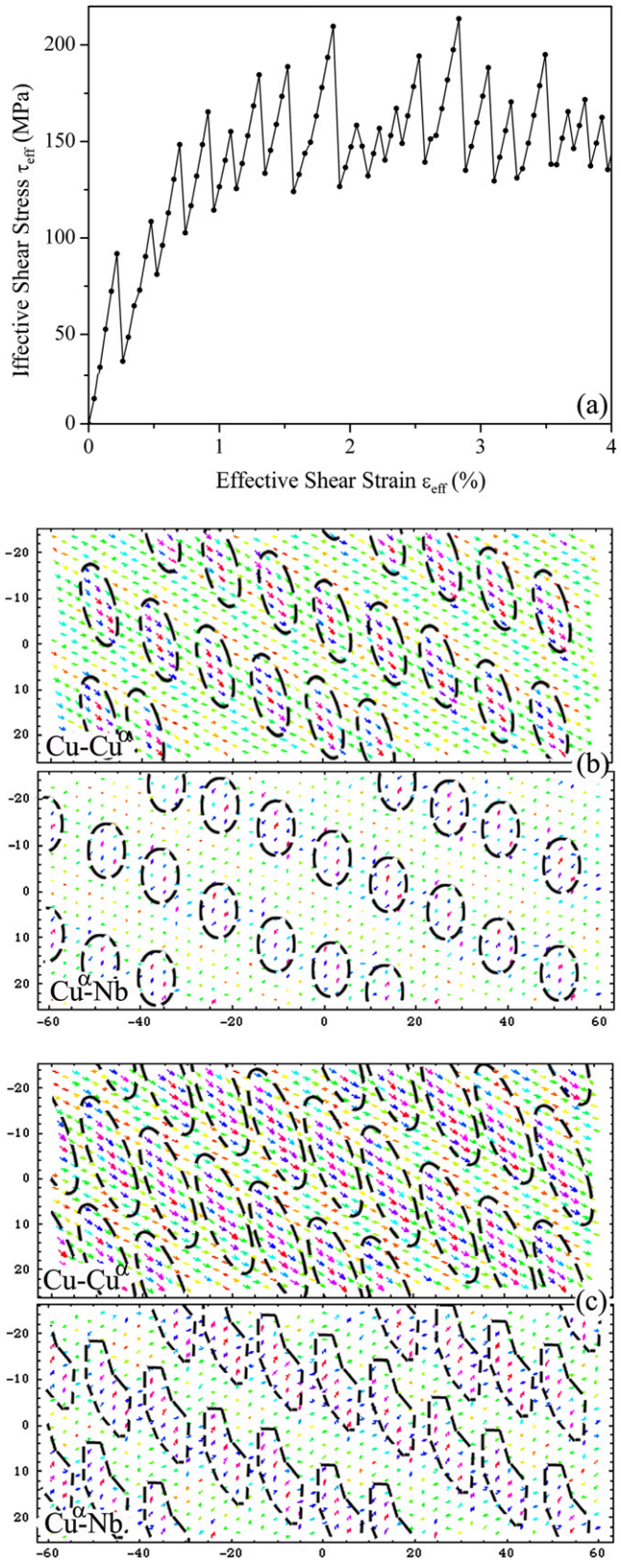

Fig. 13. Interface sliding for KS_2 for the applied shear direction $[1\,1\,\bar{2}]_{Cu}$, showing (a) the effective shear stress–strain curve, and patterns in the vector plots of disregistry corresponding to different shear strain at (b) 1.0% and (c) 1.5%. Arrows are disregistry and dashed lines represent dislocations.

the strength of layered composites and interface sliding. The spatial non-uniformity of shear strength in interfaces results in the dislocation core spreading in an intricate pattern. As shown in Fig. 14, a screw dislocation in the Cu crystal, near the interface, can be fully absorbed in the interface at zero applied stress. The dislocation core spreads in an intricate pattern within the Cu–Nb interface for KS_1, and in the two interfaces Cu–Cu$^{\alpha}$ and Cu$^{\alpha}$–Nb for KS_2. The difference of the spreading width implies that the KS_2 interface has a lower shear strength than the KS_1 interface.

Fourth, interfacial dislocation loops can nucleate at boundaries between slipped and non-slipped regions owing to the spatial non-uniformity of shear strength. With continued shearing, interface sliding occurs by glide of dislocation loops nucleated in the interface. This interfacial dislocation mechanism operates in the Cu–Nb interface for KS_1, and in the two interfaces for KS_2. The anisotropy of shear strength is ascribed to interfacial dislocations that have different characters depending on the applied shear directions.

Finally, it is worth pointing out that the shear response observed in this study of Cu–Nb interfaces could be a general feature of fcc/bcc interfaces. The shear strength of an interface not only depends on the bond strength between

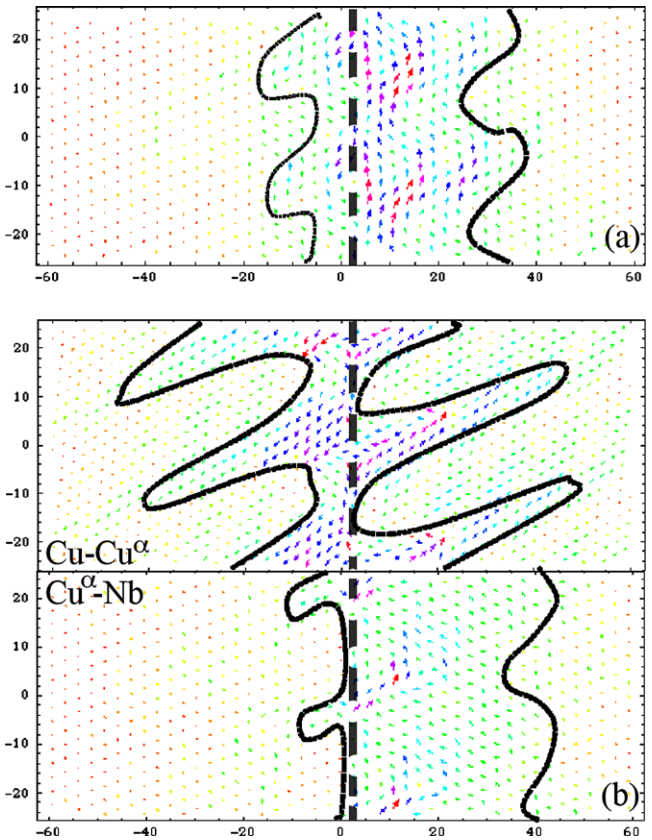

Fig. 14. Patterns in the vector plots of disregistry, showing core spreading when a full screw dislocation enters the interfaces: (a) KS_1 and (b) KS_2. The dashed line indicates the position of the screw dislocation in the interface. Cu–Cu$^{\alpha}$ is the interface between the strained interfacial Cu$^{\alpha}$ monolayer and Cu crystal; Cu$^{\alpha}$–Nb is the interface between the strained interfacial Cu$^{\alpha}$ monolayer and Nb crystal.

Cu and Nb atoms, but also on atomic arrangement of the interface which is mainly determined by the crystal structures, the crystallographic orientation relationship and the lattice misfit strain. The spatial non-uniformity of shear strength in the interface is related to the quasi-repeating pattern observed in interfaces, such as the lower shear resistance within the vortex regions in the KS_1 interface and the large displacement regions in the KS_2 interface. In addition to the lower shear resistance found for the Cu–Nb interface, the spatial non-uniformity of shear resistance is a general feature for fcc/bcc interfaces with the KS orientation relation, and can account for mechanisms of interface sliding and dislocation core spreading in these interfaces.

Acknowledgments

This work was supported by the US Department of Energy, Office of Science, Office of Basic Sciences.

References

[1] Misra A, Verdier A, Lu YC, Kung H, Mitchell TE, Nastasi M, et al. Scripta Mater 1998;39:555.
[2] Clemens BM, Kung H, Barnett SA. MRS Bull 1999;24:20.
[3] Phillips MA, Clemens BM, Nix WD. Acta Mater 2003;51:3157.
[4] Misra A, Hoagland RG, Kung H. Phil Mag 2004;84:1021.
[5] Misra A, Hirth JP, Hoagland RG, Embury JD, Kung H. Acta Mater 2004;52:2387.
[6] Anderson PM, Bingert JF, Misra A, Hirth JP. Acta Mater 2003;51:6059.
[7] Misra A, Demkowicz MJ, Zhang X, Hoagland RG. JOM 2007;59:62.
[8] Hoagland RG, Mitchell TE, Hirth JP, Kung H. Phil Mag A 2002;82:643.
[9] Hoagland RG, Kurtz RJ, Henager CH. Scripta Mater 2004;50:775.
[10] Hoagland RG, Hirth JP, Misra A. Phil Mag 2006;86:3537.
[11] Demkowicz MJ, Wang J, Hoagland RG. In: Hirth JP, editor. Dislocations in solids, vol. 14, 2008 [chapter 83]., in press, doi: 10.1016/S1572-4859.
[12] Rice JR. J Mech Phys Solid 1992;40:239.
[13] Randle V. Acta Mater 1997;46:1459.
[14] Porter DA, Eastering KE. Phase transformations in metals and alloys. 2nd ed. Boca Raton, FL: CRC Press; 1992. p. 340.
[15] Demkowicz MJ, Hoagland RG. J Nucl Mater 2007. doi:10.1016.
[16] Voter AF, Chen SP. Mater Res Soc Symp Proc 1987;82:175.
[17] Johnson RA, Oh DJ. J Mater Res 1989;4:1195.
[18] Liu CL, Cohen JM, Adams JB, Voter AF. Surf Sci 1991;253:334.
[19] Huang H, Wang J. Appl Phys Lett 2003;83:4752.
[20] Wang J, Huang H, Cale TS. Model Simul Mater Sci Eng 2004;12:1209.
[21] Henager CH, Kurtz RJ, Hoagland RG. Phil Mag A 2004;84:2277.
[22] Wang J, Hoagland RG, Misra A. J Mater Res 2008;23. doi: 10.1557/JMR.2008.0120.
[23] Vitek V. Cryst Latt Def 1974;5:1.